

Facet-dependent photocatalytic performance of TiO<sub>2</sub>: A DFT studySicong Ma<sup>a,1</sup>, Weiyu Song<sup>a,1</sup>, Bing Liu<sup>a</sup>, Wenjia Zhong<sup>a</sup>, Jianlin Deng<sup>a</sup>, Huiling Zheng<sup>a</sup>, Jian Liu<sup>a</sup>, Xue-Qing Gong<sup>b</sup>, Zhen Zhao<sup>a,\*</sup><sup>a</sup> State Key Laboratory of Heavy Oil Processing, College of Science, China University of Petroleum-Beijing, Beijing 102249, PR China<sup>b</sup> Key Laboratory for Advanced Materials, Centre for Computational Chemistry and Research Institute of Industrial Catalysis, East China University of Science and Technology, Shanghai 200237, PR China

## ARTICLE INFO

## Article history:

Received 26 February 2016

Received in revised form 3 May 2016

Accepted 9 May 2016

Available online 10 May 2016

## Keywords:

Anatase TiO<sub>2</sub>

Excited electrons transfer

CO<sub>2</sub> photoreduction

Density functional theory

Facet-dependent

## ABSTRACT

The facet-dependent photocatalytic activity of TiO<sub>2</sub> has been found in CO<sub>2</sub> photoreduction. However, which facet is more reactive and the nature of its dramatically different activity are still in the great debate. Utilizing density functional theory, two key photocatalytic steps (photo-generated electrons transfer and photoreaction) are investigated on anatase TiO<sub>2</sub> (001) and (101) facets to unravel such puzzles. The photo-generated electrons transfer (within the bulk, from bulk to surface and across the surface) has similar transfer barrier, indicating that the experimentally observed different activity may not be dominated by photo-generated electrons transfer, and the photoreaction process could be the rate-limiting step. The possible CO<sub>2</sub> photoreduction reaction paths have been extensively examined and large barrier difference on two facets is obtained. The facts that the higher conduction band minimum can generate more strongly reductive electrons, the lower reaction barrier can lead to the faster reaction rate and the product adsorption can have more suitable properties give rise to a higher activity on (101) facets than that on (001) facets.

© 2016 Elsevier B.V. All rights reserved.

## 1. Introduction

In the past few decades, photocatalytic properties of semiconducting nanocrystals with well-defined facets have been intensely studied [1]. Among the semiconductor materials, titanium dioxide (TiO<sub>2</sub>) has been undoubtedly proven to be one of the best photocatalysts due to its unique properties [2–4]. The photocatalytic performance of TiO<sub>2</sub> depends on the properties including the surface area, particle size, morphology and surface structure. Among these properties, catalytic activity largely depends on the exposed facets [5–14].

For TiO<sub>2</sub>, the anatase phase has received the most attention because of its relatively high catalytic activity and electron mobility compared to that of the rutile and brookite phases [15]. In terms of surface structure, (001) facets have been considered to be more reactive than (101) facets [16–19]. Li et al. found that photodegradation activity of methyl orange on (001) facets is 3.22 times higher than (101) facets [10]. Yu et al. considered that the photoreduction CO<sub>2</sub> activity is on the order of (101) + (001) > (001) > (101) [11].

But opposite opinions are also proposed by others. Pan et al. found the photo activity is on the order of (101) > (001) in the photooxidation and reduction reactions for generating OH radicals and hydrogen evolution, respectively [6]. The photocatalytic activity order (101) > (001) is also found in the gaseous phase for the photoreduction of CO<sub>2</sub> to CH<sub>4</sub> [13]. These contradicting experimental findings reveal the complex nature of surface termination dependent photocatalytic activity of TiO<sub>2</sub>, which will be the main focus of present contribution.

The reasons why researchers believe that (001) facets have a higher activity can be summarized as following: (1) the higher surface energy [20], 0.90 J/m<sup>2</sup> for (001) facets vs 0.44 J/m<sup>2</sup> for (101) facets, and the higher percentage of Ti<sub>5c</sub> on surface, 100% for (001) facets vs 50% for (101) facets, leading to stronger interaction with adsorbates [21–23]; (2) smaller band gap [24]; (3) higher Valence Band maximum (VBM) and Conduction Band minimum (CBM) [11]. Equally, the reasons why (101) facets have a higher activity can be concluded as: (1) The suitable CO<sub>2</sub> adsorption properties [13]; (2) Higher CBM generating more strongly reductive electrons [6,13].

Generally speaking, the photocatalytic reactions can be divided into three steps: photoexcitation, photo-generated carrier transfer and photoreaction [25]. To reply the question which facets have a higher activity, we need to know which step controls the photocatalytic reactions. Unfortunately, there is no final conclusion at

\* Corresponding author.

E-mail address: [zhenzhao@cup.edu.cn](mailto:zhenzhao@cup.edu.cn) (Z. Zhao).<sup>1</sup> These two authors contributed equally to this work.

present. Photoexcitation efficiency has been deeply studied. Band gap is considered as the benchmark to evaluate the photoexcitation efficiency [26]. For the dramatic activity difference of (101) vs. (001) facets, there must be other key factors rather than the slight bandgap difference. For the photo-generated carrier transfer, the previous results can be summarized as: (1) the barriers of bulk excited electron transfer and bulk hole transfer are around 0.3 eV and 0.55 eV, respectively [27–29]; (2) the barriers for hole and excited electron transfer on the surface are larger than that in the bulk for rutile (110) facets [27]. To our best knowledge, there is not yet theoretical work dedicated to anatase (101) and (001) facets regarding the photo-generated carrier transfer process on the surface. Regarding the photoreaction, one of the most interesting reactions is CO<sub>2</sub> photoreduction, which can produce raw materials and valuable chemicals. Experimentally, the reaction has been shown to be sensitive to the exposed facets of TiO<sub>2</sub>. There are some systematic works about CO<sub>2</sub> reduction on TiO<sub>2</sub> (101) facets [30,31], so we would pay more attention to CO<sub>2</sub> reduction on TiO<sub>2</sub> (001) facets.

In the present contribution, we will employ density functional theory method on anatase TiO<sub>2</sub> (101) and (001) facets to study the photo-generated electrons transfer and the CO<sub>2</sub> photoreduction, respectively. The result is expected to provide an answer to the nature of the different activity on different facets.

## 2. Computational details

Bulk anatase TiO<sub>2</sub> forms a tetragonal lattice with space group I4<sub>1</sub>/AMD and experimental lattice constants are:  $a=b=3.776$  Å,  $c=9.486$  Å. We built a periodic slab with six and five layers for (101) and (001) facets, respectively.  $2 \times 2$  surface unit cells were used. The models contain 72 atoms for (101) facets and 60 atoms for (001) facets. We fixed the bottom two layers of Ti and O. The vacuum gap thickness was set to be 12 Å. Models of two facets are shown in Fig. 1.

All calculations were performed with code VASP using the GGA-PBE exchange-correlation potential [32]. The valence electrons (3p, 4s, 3d for Ti; 2s, 2p for C; 2s, 2p for O and 1s for H) are expanded in a plane-wave basis set within a cutoff of 400 eV. The PAW method was used to describe the effect of core electrons [33,34]. Gamma centered k-point meshes of  $2 \times 2 \times 1$  were used. We have chosen several structural optimizations and tested the variation of energy under different convergence criterion, 0.02 vs. 0.05 eV/Å, see Table S1. We found that there is little difference when increasing the convergence criterion to 0.02 eV/Å. So all structures were relaxed until the forces acting over each atom were smaller than 0.05 eV/Å. Transition states along the reaction pathways are searched by the Climbing Image Nudged Elastic Band (CI-NEB) approach [35,36]. Dipole corrections have been added along the z direction. Adsorption energies have been calculated using the formula:

$$E_{\text{ads}} = E_{\text{surf-X}} - (E_{\text{surf}} + E_{\text{X}})$$

where  $E_{\text{surf-X}}$  is the total energy of the combined system (the adsorbate X bound to the substrate),  $E_{\text{surf}}$  is the energy of the substrate alone, and  $E_{\text{X}}$  is the total energy of the adsorbate in the gas phase.

It is well known that GGA functional underestimates band gap and also tends to favor delocalized electron solutions. The method for determining the polaron structures involved adding an extra electron to surface while employing the DFT+U [37] level of theory, and then allowing the systems to relax in response to this extra electron. This relaxed system can effectively model the polaron structure. To correctly localize the added electron on the 3d orbital of Ti, DFT+U technique was employed in the present study. Within the DFT+U framework, there is no way to predict a “correct” value of U that will match every property. To localize an electron on a

3d transition metal, a large U value is needed to overcome the tendency of the excited electron to delocalize due to self-interaction errors. Deskins et al. showed that a U value near 10 eV gives band gaps in satisfactory accord with experiment for anatase TiO<sub>2</sub> [28]. A similar value of U was obtained by Persson and da Silva [38]. Moreover, we tested the stability of electron localized at different sites by  $U=4.2$  eV, see Supporting information Fig. S1. It can be found there is no difference in the variation trend of energy but only a slightly difference is found in numerical value. So we added the  $U=10$  eV correction to the 3d orbital of Ti in Section 3.1. But it has been shown that the  $U=10$  will cause deviation in describing the CO<sub>2</sub> adsorption energies (see Table S2), compared with the results of Mino et al. [22] who utilized the hybrid PBE0 functional. Tested without any U value, the CO<sub>2</sub> adsorption energies is same as the results of Mino et al. Moreover,  $U=4$  eV has been tested by Ji et al., there is little difference in the results using GGA and GGA+U [31]. Considering the above two points, we decided not to add U in the calculation of the reaction part.

To simulate the excited electron, one electron was added to the system in Section 3.1, which has been extensively used [27,28,39]. In Section 3.2, with the aim to investigate the reaction, a hydrogen atom is introduced on the surface bridging O<sub>2c</sub> atom to become a proton with an apparent charge state of +1. The electron from this H atom redistributes over Ti atoms to populate the bottom of the TiO<sub>2</sub> CB [30,40,41]. This electron mimics a photoexcited electron in these reactions.

## 3. Results and discussion

### 3.1. The transfer of excited electrons

The added electron to the surface reduces one Ti<sup>4+</sup> to Ti<sup>3+</sup>. This can be found directly by analyzing the spin magnetic moment from the calculation output of VASP code. For Ti<sup>4+</sup>, no unpaired electron exists on Ti, thus 0 μB for its spin magnetic moment. With one electron on Ti, nearly 1 μB for its spin magnetic moment suggests the existence of Ti<sup>3+</sup>. To investigate the excited electron transfer, two aspects must be considered: (1) the preferable sites to localize the excited electron, bulk or surface? (2) the barrier of excited electrons transfer. At first, we need to determine the reference state (surface state and bulk state). We tested a thicker ten layers (101) slab with fixing the bottom two layers and localized the electron at different layer, see Fig. S2. When the electron is localized below the third layer for (101) facets, the energy change is very small, nearly 0.05 eV, see Fig. S2. So the third layer Ti atom is defined as the bulk Ti atom for (101) facets. Similarly, for the (001) facets, when the electron is localized below the second layer, the energy change is very small, nearly 0.02 eV, see Fig. S3. So the second layer Ti atom is defined as the bulk Ti atom for (001) facets.

#### 3.1.1. The stability of the excited electrons

For the first question, different sites have been extensively examined to find the most preferable site to localize the excited electron. The results are shown in Table 1. It can be found that the energy of electron staying in bulk, relative to the energy of electron staying on surface, is 0.16 eV and 0.38 eV higher for (101) and (001) facets, respectively. The energy that Ti<sup>3+</sup> appears in bulk is higher than that on surface. It can be concluded that the excited electron prefers to stay on the surface than in the bulk.

The physical process to inject an excited electron to Ti is basically putting one electron to the CB of Ti. Accordingly the CBM can represent the stability of this excited electron. The DOS results of Ti at different sites for (001) facets can be found in Fig. 2 (The DOS of (101) facets can be found in Fig. S4), the CBM for Ti on surface is lower than that in bulk, which is directly related to different coor-

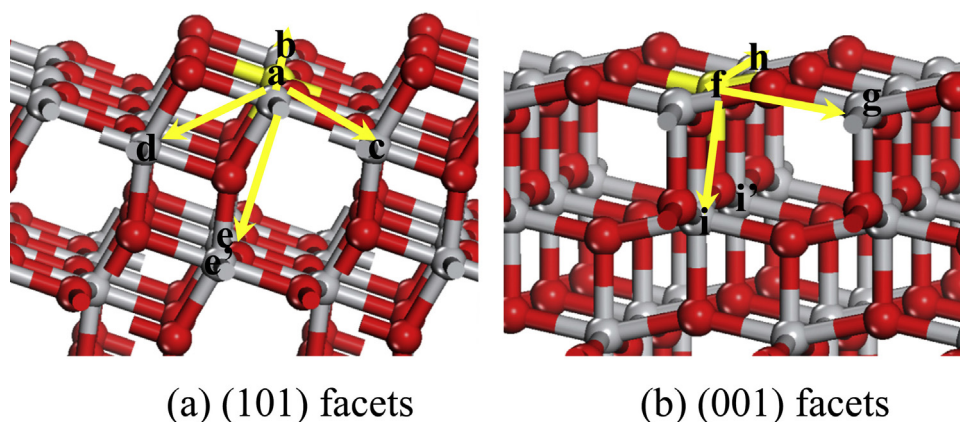


**Fig. 1.** The models of (101) and (001) facets. a, b, f, h and g represent surface  $\text{Ti}_{5c}$ . c and d represent surface  $\text{Ti}_{6c}$ . e, e', i and i' represent subsurface  $\text{Ti}_{6c}$ . All letters represent the possible positions that the localized electron may appear. The localized electron moves along the directions indicated by the arrows. Red and gray, atoms depict oxygen atoms and Ti atoms, respectively (for interpretation of the references to colour in this figure legend, the reader is referred to the web version of this article).

**Table 1**

The relative energy of different  $\text{Ti}^{3+}$  positions which are labeled in Fig. 1 for different facets. The energy of  $\text{Ti}^{3+}$  at b, c, d, e, e' is relative to the energy of  $\text{Ti}^{3+}$  at a for (101) facets, and the energy of  $\text{Ti}^{3+}$  at g, h, i, i' is relative to the energy of  $\text{Ti}^{3+}$  at f for (001) facets.

Facets	Position of $\text{Ti}^{3+}$	Coordination number of Ti	Relative Energy/eV
(101)	a	5	0
	b	5	0
	c	6	0.2
	d	6	0.2
	e	6	0.16
	e'	6	0.16
(001)	f	5	0
	g	5	0
	h	5	0
	i	6	0.38
	i'	6	0.38

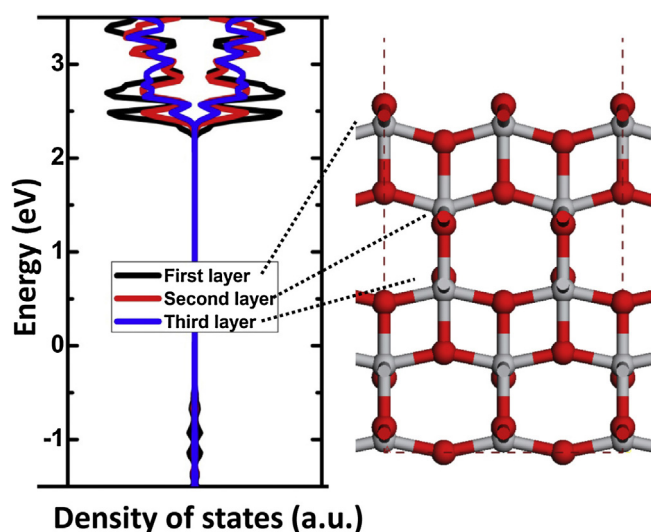


**Fig. 2.** Density of states of different Ti positions for (001) facets and (101) facets model, the layer numbered from top to bottom.

coordination number of Ti [42]. This explains the above result that the excited electron prefers to localize on surface than in bulk.

### 3.1.2. The barrier of excited electron transfer

For the second question, to estimate the barrier of electron transfer on (101) and (001) facets, we computed the potential energy profiles for a series of linearly interpolated geometries

$$X(a) = a \times X(A) + (1 - a) \times X(B)$$

where  $a$  ( $0 < a < 1$ ) is the reaction coordinate and  $X(A)$  is the optimized geometries of  $\text{Ti}^{3+}$  and  $X(B)$  is the optimized geometries of another  $\text{Ti}^{3+}$ . The results are summarized in Fig. 3. For the  $\text{TiO}_2$  (101) facets, the transfer barriers of electron in bulk, from bulk to surface and from surface to surface are 0.29, 0.37 and 0.45 eV, respectively. For (001) facets, they are 0.33, 0.20 and 0.48 eV. Our result is close to the results of Deskins et al. whose transfer barrier in bulk is 0.3 eV for anatase  $\text{TiO}_2$  [28]. So the barrier is in the order of

$$E_{a}^{\text{Bulk} \rightarrow \text{Bulk}} < E_{a}^{\text{Surface} \rightarrow \text{Surface}} < E_{a}^{\text{Surface} \rightarrow \text{Bulk}}$$

Combined the stability with the transfer barrier, the excited electrons tend to transfer from bulk to surface with a low transfer barrier. Once the electrons get to the surface, they may transfer on surface or to reactant, alternatively, which is decided by the transfer barrier.

In the following, we will compare (001) facets with (101) facets to find the difference regarding the electron localization and its transfer. For the relative stability of electron on both facets, because the energy that  $\text{Ti}^{3+}$  appears in the bulk should be identical for both facets, we chose this energy as the reference to evaluate the energy that  $\text{Ti}^{3+}$  appeared on surface. It can be found that the energy that  $\text{Ti}^{3+}$  appears at (001) facets is 0.22 eV lower than that at (101) facets, indicating (101) facets have a higher CBM which may generate more strongly reductive electrons.

Moreover, the barriers of surface electron transfer are close for both facets, around 0.46 eV, meaning the similar rate of electron transfer. Considering the experimentally observed dramatically different activity for different photoreaction on the two facets, it would be reasonable to speculate that the chemical reaction process is the rate-limiting step, which will be studied in the coming section.

### 3.2. $\text{CO}_2$ photoreduction via a proton-assisted two electron transfer reaction

It is well known that the transfer of a single electron to  $\text{CO}_2$  has a very unfavorable redox potentials,  $E_{\text{CO}_2^-/\text{CO}_2} = -1.9\text{ eV}$ . The situation is better for a proton-assisted transfer of multiple electrons [43]. Overall reactions to produce CO, HCOOH, HCHO,  $\text{CH}_3\text{OH}$ , and

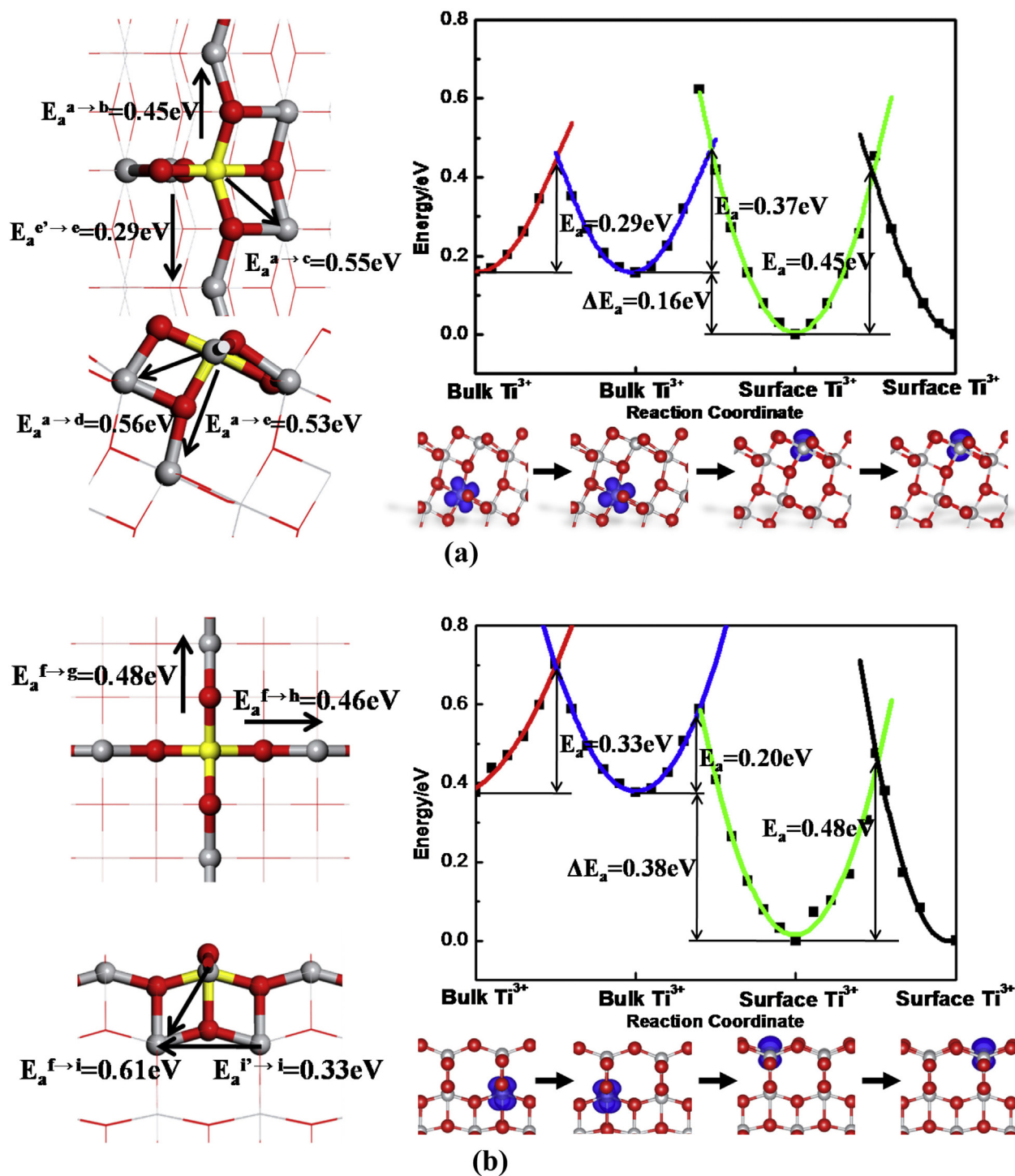


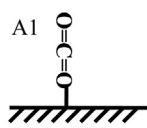
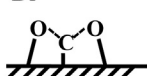
**Fig. 3.** The different directions of electron transfer and the transfer barrier for (a) (101) facets and (b) (001) facets. O atoms are in red and Ti in gray. The isosurface ( $0.04 \text{ e}/\text{\AA}^3$ ) of calculated spin charge densities are in dark blue (for interpretation of the references to colour in this figure legend, the reader is referred to the web version of this article).

$\text{CH}_4$  need 2, 2, 4, 6 and 8 electrons, respectively. The initial activation of  $\text{CO}_2$  is the rate limiting step [30]. The reactions step then proceed step by step [11]. That means the initial proton-assisted two electron transfer reaction to produce CO or HCOOH is very important. So the proton-assisted two electron transfer reaction from  $\text{CO}_2$  to CO or HCOOH would be employed to study the facet dependent of  $\text{CO}_2$  reduction.

The adsorption of  $\text{CO}_2$  is first studied. There are different adsorption configurations. The most stable adsorption configuration of  $\text{CO}_2$  on the (101) facets is vertically adsorbed on top of  $\text{Ti}_{5c}$  atom,

labeled as A1 configuration, and the most stable adsorption configuration on (001) facets has two O atoms bridging two 5-fold Ti atoms and a C atom pointing downward forming a bond with the  $\text{O}_{2c}$  atom, labeled as B1 configuration [22,23]. Because  $\text{CO}_2$  reduction reaction to CO or HCOOH needs two electrons which means that  $\text{CO}_2$  must be adsorbed on a negatively charged site, so the adsorption of  $\text{CO}_2$  on anion surface introducing two electrons by two hydrogen atoms is also calculated. The results are summarized in Fig. 4.



		Neutral	Anion(2H)	Reference <sup>a</sup> Neutral	
(101) facets	A1	-0.15	-0.12	-0.34	
	B1	0.37	0.22	0.32	
(001) facets	A1	-0.25	0.02	-0.23	
	B1	-1.34	-0.38	-1.31	

**Fig. 4.** The adsorption energy (eV) of CO<sub>2</sub> with different adsorption configurations on different facets and the sketch map of the adsorption configurations, <sup>a</sup>Ref. [22].

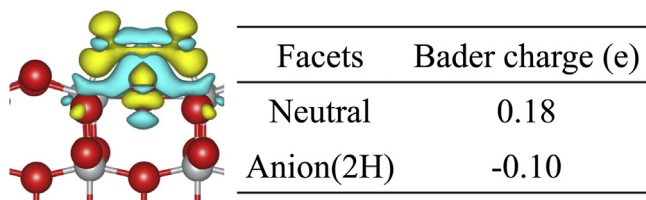


**Fig. 5.** The Charge density difference of CO<sub>2</sub> adsorbing on neutral (001) facets as defined by:  $\Delta\rho = \rho_{\text{surf-CO}_2} - \rho_{\text{CO}_2} - \rho_{\text{surf}}$  and the Bader Charges of CO<sub>2</sub>. The yellow and green area represents electron accumulation and depletion, respectively.

For the neutral surface, the results are consistent with others [22]. For the anion surface, it is noteworthy that the adsorption energy is smaller than that on the neutral surface. Charge density difference and Density of State (DOS) analysis are performed to understand the origin of different adsorption energy, see Fig. 5. It can be found that the electron would transfer from CO<sub>2</sub> to support, meaning that the more electrons on the surface would be unfavorable for CO<sub>2</sub> adsorption.

He et al. [30] have been systematically investigated the CO<sub>2</sub> photoreduction to CO and HCOOH on anatase TiO<sub>2</sub> (101) facets. They believed that CO<sub>2</sub> tends to be reduced to HCOOH via A1 configuration. So here we will only consider CO<sub>2</sub> reduction to HCOOH via A1 configuration on (101) facets.

Nørskov et al. [44] proposed that there is thus only a narrow range of adsorption energy differences in which two species can be co-adsorbed on the surface in appreciable amounts. As soon as one species binds about 0.2 eV stronger than all other species, it will dominate the surface at room temperature. Therefore we believed that CO<sub>2</sub> B1 configuration would dominate on (001) facets according to the large adsorption energy difference. So the B1 con-

figuration for (001) facets are chosen for the following mechanism study.

### 3.2.1. The reaction pathways of CO<sub>2</sub> to HCOOH on (101) facets

The potential energy diagram with intermediate structures via A1 configuration on (101) facets is shown in Fig. 6. The reaction pathway can be written as:



The first step is the adsorption of CO<sub>2</sub> (state ii, Fig. 6) with a binding energy of 0.12 eV. The distance of CO<sub>2</sub> molecule to the support is 2.86 Å and the bond lengths of CO<sub>2</sub> are very close to that in gas phase, consistent with the weak binding interaction. Then CO<sub>2</sub> gets closer to surface accompanied with the formation of Ti–O bond, and interacts with H atom that transfers from O<sub>2c</sub> atom to C atom forming the HCO<sub>2</sub> (state iii, Fig. 6). This reaction step has an activation barrier of 1.27 eV and an exothermic reaction energy of 0.17 eV. The transition state (TS) with CO<sub>2</sub> bent at slightly larger angle of 136.7° is in a monodentate configuration having one strong Ti–O bond with a bond length of 2.04 Å. The bond distance between the C atom and the H atom is 1.58 Å. After that, HCO<sub>2</sub> can rotate itself to let the oxygen of carbonyl group get closer to the second H atom to form the HCOOH (state iv, Fig. 6). We have used CI-NEB method to find the transition state from HCOO to HCOOH. The potential energy curve gradually declined, and did not appear the saddle point. According to the results of He et al. and Ji et al. [30,31], the reaction barrier from HCOO to HCOOH is only 0.01 eV, indicating such process is very easy. This reaction step has an exothermic reaction energy of 0.61 eV. It takes 0.79 eV to desorb formic acid into the gas phase. The desorption energy is close to the results of Vittadini et al. which is 0.92 eV for the molecular monodentate adsorption configuration of HCOOH [45]. The rate-limiting step is the activation of CO<sub>2</sub> via the H atom with an reaction barrier of 1.27 eV.

### 3.2.2. The reaction pathways of CO<sub>2</sub> to HCOOH and CO on (001) facets

Regarding the first step of CO<sub>2</sub> activation on (001) surface, two possible paths exist for its combination with H atoms which will lead to quite different products, one to formic acid (named as formic acid pathway in the following), the other one to CO and H<sub>2</sub>O (named as CO pathway in the following). We will examine the two possible pathways in the coming section respectively.

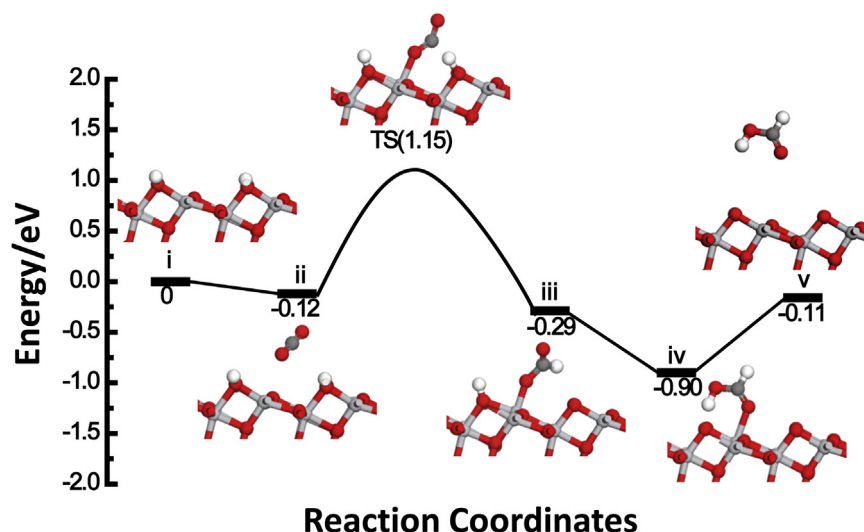


**Fig. 6.** Complete reaction energy diagram for CO<sub>2</sub> reduction to formic acid on (101) facets. White and dark gray atoms depict H, and C atoms, respectively.

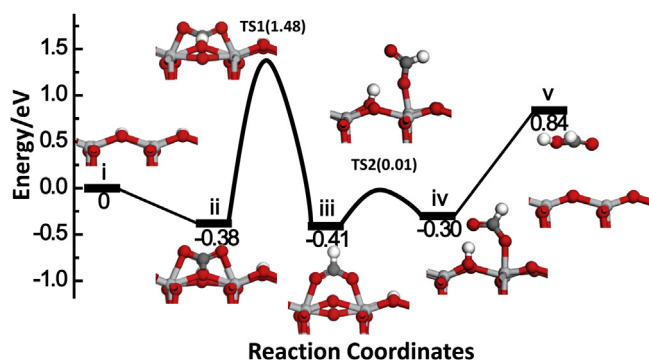
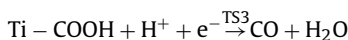
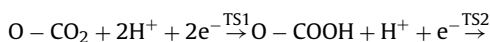


Fig. 7. The reaction energy diagram for CO<sub>2</sub> reduction to HCOOH on (001) facets.

The potential energy diagram with all intermediate structures via formic acid pathway on (001) facets is shown in Fig. 7. The first step is the adsorption of CO<sub>2</sub> (state ii, Fig. 7) with a binding energy of 0.38 eV. The distances of Ti–O and C–O<sub>2c</sub> bonds are 2.17 Å and 1.36 Å, respectively. The C atom gets closer to H atom to form the HCO<sub>2</sub> (state iii, Fig. 7) accompanied with the cleavage of H–O<sub>2c</sub> and C–O<sub>2c</sub> bonds and the formation of H–C bond. In the state iii, the distances of the two Ti–O bonds are shortened to 2.09 Å. This reaction step has an activation barrier of 1.86 eV and an exothermic reaction energy of 0.03 eV. The TS has a similar structure with state ii, CO<sub>2</sub> bent angle is 122.4° vs 133.2° in state ii. The bond distance between the C atom and the H atom is 1.43 Å. After that, the HCO<sub>2</sub> changes the adsorption configuration by breaking one of the Ti–O bond and rotated itself to lead to the oxygen of carbonyl group getting closer to the second H atom (state iv, Fig. 7). The configuration transformation barrier is 0.42 eV and the transformation process has an endothermic reaction energy of 0.09 eV. The structure of state iv is same as the dissociated adsorption configuration of HCOOH. So the dissociated species can recombine together forming HCOOH and desorb from surface. The desorption energy is 1.14 eV consistent with others whose results is 1.19 eV [46].

For the CO pathway, the potential energy diagram is shown in Fig. 8. The whole reaction can be written as:



The first step is the adsorption of CO<sub>2</sub> (state ii, Fig. 8) with a binding energy of 0.38 eV. Then the O atom gets closer to H atom to form the COOH (state iii, Fig. 8) accompanied with the cleavage of H–O<sub>2c</sub> bond and the formation of hydroxyl group. This reaction step has an activation barrier of 1.17 eV and an endothermic reaction energy of 0.98 eV. After that, breaking C–O<sub>2c</sub> and Ti–O bonds, COOH migrates to another adsorption sites forming a new adsorption configuration (state iv, Fig. 8), where C atom bonds with Ti atom and the oxygen of carbonyl group bonds with another Ti atom. The migration barrier is 0.93 eV. Then the new adsorption configuration can swing hydroxyl group to let the second H atom transfer to the oxygen of hydroxyl group, and generate CO and H<sub>2</sub>O (state v, Fig. 8). In this state, CO and H<sub>2</sub>O are physically adsorbed on surface. The distances of CO and H<sub>2</sub>O molecules to the support are 2.37 Å and 1.77 Å. This process has an activation barrier of 0.93 eV and an endothermic reaction energy of 0.69 eV. Finally it takes 0.43 eV to desorb CO and H<sub>2</sub>O into the gas phase.

To facilitate comparison with others, the activation barriers of rate limiting step are collected in Table 2 for different facets. The barrier for CO<sub>2</sub> reduction to formic acid for (101) facets is calculated to be 1.27 eV, which is much larger than that reported by He et al. [30]. Such difference can be attributed to the model size, 2 × 1

supercell, which has been pointed out by Ji et al. [31]. The small supercell leads to underestimate the barriers for the CO<sub>2</sub> photoreduction. To ensure that our model size is large enough, we compare our results with the results reported by Ji et al. who have used a 3 × 1 supercell containing 180 atoms, see Fig. S5 [31]. It can be found that there is little difference in the two cases, indicating that our model is large enough for simulating the occurrence of reaction. Moreover, for TiO<sub>2</sub> (001) facets, although the reaction barrier of CO pathway is smaller than that of formic acid pathway, the apparent energy needs from environment for CO pathway (1.71 eV, Fig. 8) is quite larger than that of formic acid pathway (1.48 eV, Fig. 7). So the formic acid pathway is the dominant pathway on (001) facets. For the (101) and (001) facets, the difference of apparent energy needs to overcome the reaction barrier is 0.33 eV. A large barrier difference, around 0.3 eV, may lead to huge rate difference, 1 × 10<sup>5</sup> times (300 K). So it can be concluded that the reaction rate follows the order:  $r_{101} \gg r_{001-\text{HCOOH}} \gg r_{001-\text{CO}}$ .

Combined the photo-generated electrons transfer with photoreaction, the following conclusions can be drawn, which supports the opinion that the (101) facets have a higher activity than (001) facets:

- (1) Despite the similar barriers of surface electron transfer for both facets, the energy that Ti<sup>3+</sup> appeared on (001) facets is 0.22 eV lower than that at (101) facets. It suggests that the reductive ability of electrons generated on (101) facets is higher than that on (001) facets, which can be transferred more easily to reactants, consistent with experimental results [6,13].
- (2) The barrier of chemical reaction step is much higher than the barrier of excited electron transfer, suggesting that reaction step is the rate-limiting step. The reaction rate is in the order of  $r_{101} \gg r_{001-\text{HCOOH}} \gg r_{001-\text{CO}}$  further supporting that (101) facets have a higher activity.
- (3) On the (101) facets, formic acid remains undissociated [45]. In contrast, formic acid adsorbs dissociatively on the (001) facets, the adsorption energies are around 0.2 eV higher than those of water, which means that formic acid is able to replace water adsorbed at the anatase surface [46]. The existence of formic acid on surface may occupy the active site and inhibit the reaction. More suitable product adsorption properties further prove that (101) facets have a higher activity.

#### 4. Conclusions

Density functional theory method is employed to study the transfer of excited electron and the proton-assisted two electron transfer CO<sub>2</sub> photoreduction reaction on TiO<sub>2</sub> (101) and (001) facets with the aim to elucidate the facets dependent photocatalytic activity of TiO<sub>2</sub> catalyst. For the excited electron transfer, stability and transfer barrier are considered. The excited electron prefers to stay on surface than in bulk for both facets. The energy of Ti<sup>3+</sup> appeared on (001) facets is lower than that on (101) facets indicating (101) facets have a higher CBM. The barriers of excited electron transfer within bulk and across surface are similar for both facets. For the proton-assisted two electron transfer CO<sub>2</sub> photoreduction reaction, CO<sub>2</sub> to CO or HCOOH has been investigated. CO<sub>2</sub> tends to generate HCOOH and the reaction barrier on (101) facets is lower than the barrier on (001) facets. For the product, formic acid remains undissociated on (101) facets and formic acid adsorbed dissociatively on the (001) surface. The higher CBM generating more strongly reductive electrons, the lower barrier leading faster reaction rate and the more suitable formic acid adsorption properties are the reason why (101) facets have a higher activity.

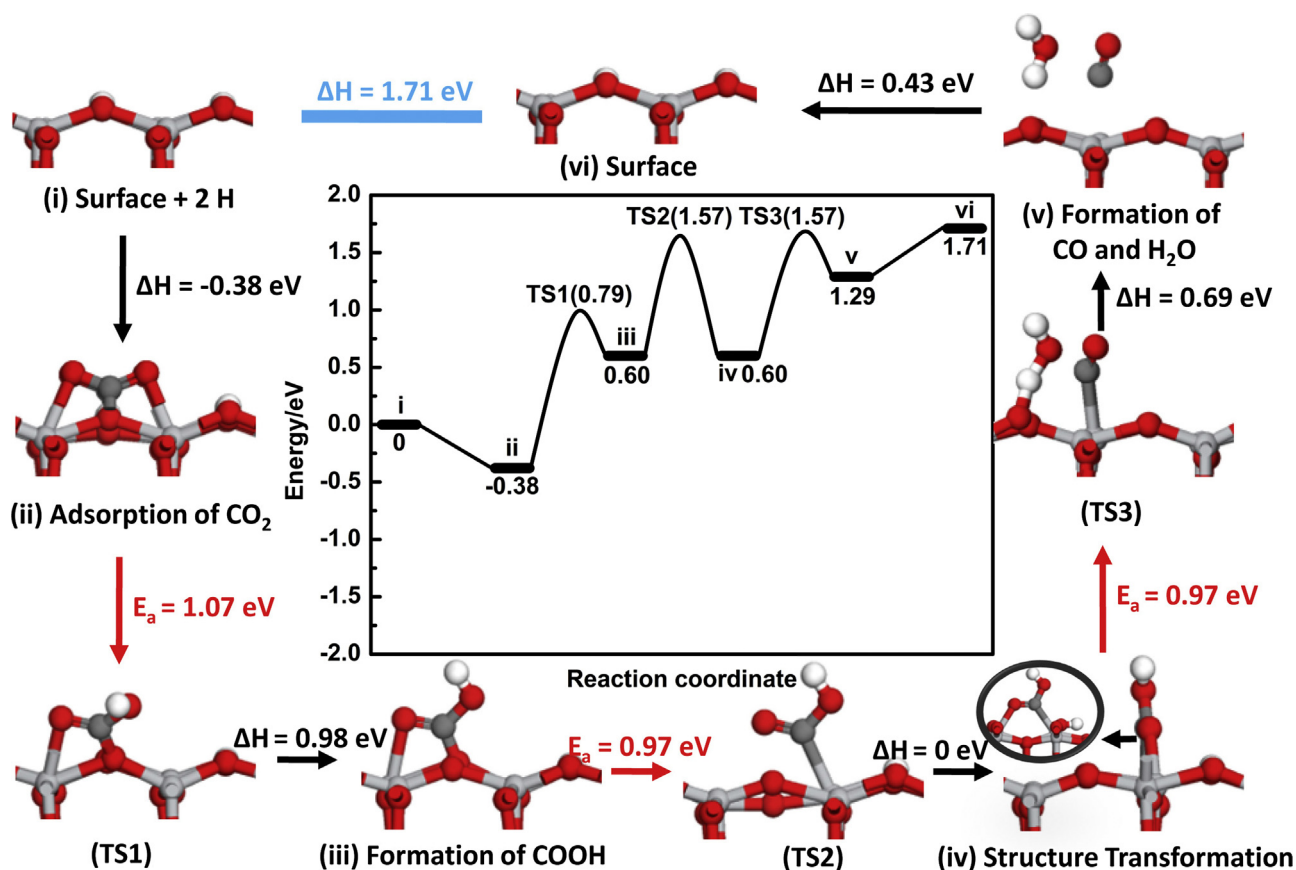


Fig. 8. The reaction energy diagram for CO<sub>2</sub> reduction to CO on (001) facets.

**Table 2**

The activation barrier of rate limiting step for CO<sub>2</sub> to HCOOH or CO.

	Systems	Methods	Activation Barrier/eV	References
CO <sub>2</sub> → HCOOH	Anatase TiO <sub>2</sub> (101)	PBE	1.27	This work
	Anatase TiO <sub>2</sub> (101)	PBE	1.15	[31]
	Anatase TiO <sub>2</sub> (101)	PBE	0.56	[30]
	Anatase TiO <sub>2</sub> (101)	PBE+U(4)/HSE	1.49	[31]
	Anatase TiO <sub>2</sub> (001)	PBE	1.86	This work
CO <sub>2</sub> → CO	Rutile TiO <sub>2</sub> (110)	PBE-D3+solvation effect	1.22	[47]
	Anatase TiO <sub>2</sub> (001)	PBE	1.17	This work
	Anatase TiO <sub>2</sub> (101)	PBE	0.47	[30]
	Anatase TiO <sub>2</sub> (101)	PBE+U(4)/HSE	1.41	[31]
	Anatase TiO <sub>2</sub> (101)	PBE	1.07	[31]
	Anatase TiO <sub>2</sub> (101)	PBE	1.07	[31]

## Acknowledgements

We acknowledge financial support for this research from 973 program of China (no. 2012CB215001), China University of Petroleum-Beijing (no. 2462015YJRC005) and the National Natural Science Foundation of China (nos. 21503273, 21477164). Computing time in the National Super Computing Center in Jinan is acknowledged.

## Appendix A. Supplementary data

Supplementary data associated with this article can be found, in the online version, at <http://dx.doi.org/10.1016/j.apcatb.2016.05.017>.

## References

- [1] S.N. Habisreutinger, L. Schmidt-Mende, J.K. Stolarczyk, *Angew. Chem. Int. Ed.* 52 (2013) 7372–7408.
- [2] H. Zhang, J.F. Banfield, *Chem. Rev.* 114 (2014) 9613–9644.
- [3] G. Liu, H.G. Yang, J. Pan, Y.Q. Yang, G.Q. Lu, H.-M. Cheng, *Chem. Rev.* 114 (2014) 9559–9612.
- [4] F. De Angelis, C. Di Valentin, S. Fantacci, A. Vittadini, A. Selloni, *Chem. Rev.* 114 (2014) 9708–9753.
- [5] N. Roy, Y. Park, Y. Sohn, K.T. Leung, D. Pradhan, *ACS Appl. Mater. Interfaces* 6 (2014) 16498–16507.
- [6] J. Pan, G. Liu, G.Q.M. Lu, H.M. Cheng, *Angew. Chem. Int. Ed.* 50 (2011) 2133–2137.
- [7] J. Mao, L. Ye, K. Li, X. Zhang, J. Liu, T. Peng, L. Zan, *Appl. Catal. B-Environ.* 144 (2014) 855–862.
- [8] L. Ye, J. Liu, L. Tian, T. Peng, L. Zan, *Appl. Catal. B-Environ.* 134 (2013) 60–65.
- [9] Q. Xu, J. Yu, J. Zhang, J. Zhang, G. Liu, *Chem. Commun.* 51 (2015) 7950–7953.
- [10] C. Li, C. Koenigsmann, W. Ding, B. Rudsteyn, K.R. Yang, K.P. Regan, S.J. Konezny, V.S. Batista, G.W. Brudvig, C.A. Schmuttenmaer, *J. Am. Chem. Soc.* 137 (2015) 1520–1529.
- [11] J. Yu, J. Low, W. Xiao, P. Zhou, M. Jaroniec, *J. Am. Chem. Soc.* 136 (2014) 8839–8842.
- [12] X. Ma, Y. Dai, M. Guo, B. Huang, *Langmuir* 29 (2013) 13647–13654.
- [13] L. Ye, J. Mao, T. Peng, L. Zan, Y. Zhang, *Phys. Chem. Chem. Phys.* 16 (2014) 15675–15680.

- [14] J. Yu, L. Qi, M. Jaroniec, *J. Phys. Chem. C* 114 (2010) 13118–13125.
- [15] C. Howard, T. Sabine, F. Dickson, *Acta Crystallogr. B* 47 (1991) 462–468.
- [16] J. Yu, G. Dai, Q. Xiang, M. Jaroniec, *J. Mater. Chem.* 21 (2011) 1049–1057.
- [17] X. Han, Q. Kuang, M. Jin, Z. Xie, L. Zheng, *J. Am. Chem. Soc.* 131 (2009) 3152–3153.
- [18] S. Liu, J. Yu, M. Jaroniec, *J. Am. Chem. Soc.* 132 (2010) 11914–11916.
- [19] H.G. Yang, C.H. Sun, S.Z. Qiao, J. Zou, G. Liu, S.C. Smith, H.M. Cheng, G.Q. Lu, *Nature* 453 (2008) 638–641.
- [20] M. Lazzeri, A. Vittadini, A. Selloni, *Phys. Rev. B* 63 (2001) 155409.
- [21] C. Sun, L.-M. Liu, A. Selloni, G.Q.M. Lu, S.C. Smith, *J. Mater. Chem.* 20 (2010) 10319–10334.
- [22] L. Mino, G. Spoto, A.M. Ferrari, *J. Phys. Chem. C* 118 (2014) 25016–25026.
- [23] H. He, P. Zapol, L.A. Curtiss, *J. Phys. Chem. C* 114 (2010) 21474–21481.
- [24] Y.-F. Li, Z.-P. Liu, L. Liu, W. Gao, *J. Am. Chem. Soc.* 132 (2010) 13008–13015.
- [25] Y. Ma, X. Wang, Y. Jia, X. Chen, H. Han, C. Li, *Chem. Rev.* 114 (2014) 9987–10043.
- [26] C. Burda, Y. Lou, X. Chen, A.C. Samia, J. Stout, J.L. Gole, *Nano Lett.* 3 (2003) 1049–1051.
- [27] N.A. Deskins, M. Dupuis, *J. Phys. Chem. C* 113 (2008) 346–358.
- [28] N.A. Deskins, M. Dupuis, *Phys. Rev. B* 75 (2007) 195212.
- [29] Y.-F. Li, A. Selloni, *J. Am. Chem. Soc.* 135 (2013) 9195–9199.
- [30] H. He, P. Zapol, L.A. Curtiss, *Energy Environ. Sci.* 5 (2012) 6196–6205.
- [31] Y. Ji, Y. Luo, *ACS Catal.* 6 (2016) 2018–2025.
- [32] J.P. Perdew, K. Burke, M. Ernzerhof, *Phys. Rev. Lett.* 77 (1996) 3865.
- [33] P.E. Blöchl, *Phys. Rev. B* 50 (1994) 17953.
- [34] G. Kresse, D. Joubert, *Phys. Rev. B* 59 (1999) 1758.
- [35] G. Henkelman, B.P. Uberuaga, H. Jónsson, *J. Chem. Phys.* 113 (2000) 9901–9904.
- [36] G. Henkelman, H. Jónsson, *J. Chem. Phys.* 113 (2000) 9978–9985.
- [37] A. Liechtenstein, V. Anisimov, J. Zaanen, *Phys. Rev. B* 52 (1995) R5467.
- [38] C. Persson, A. Ferreira da Silva, *Appl. Phys. Lett.* 86 (2005) 231912.
- [39] D. Liu, L. Li, Y. Gao, C. Wang, J. Jiang, Y. Xiong, *Angew. Chem. Int. Ed.* 54 (2015) 2980–2985.
- [40] H.H. Kristoffersen, U. Martinez, B. Hammer, *Top. Catal.* 57 (2014) 171–176.
- [41] Y. Ji, Y. Luo, *J. Phys. Chem. C* 118 (2014) 6359–6364.
- [42] R.A. Van Santen, M. Neurock, *Molecular Heterogeneous Catalysis: A Conceptual and Computational Approach*, John Wiley & Sons, 2009.
- [43] P. Liao, E.A. Carter, *Chem. Soc. Rev.* 42 (2013) 2401–2422.
- [44] J.K. Nørskov, F. Studt, F. Abild-Pedersen, T. Bligaard, *Fundamental Concepts in Heterogeneous Catalysis*, John Wiley & Sons, 2014.
- [45] A. Vittadini, A. Selloni, F. Rotzinger, M. Grätzel, *J. Phys. Chem. B* 104 (2000) 1300–1306.
- [46] X.-Q. Gong, A. Selloni, A. Vittadini, *J. Phys. Chem. B* 110 (2006) 2804–2811.
- [47] W.-J. Yin, M. Krack, B. Wen, S.-Y. Ma, L.-M. Liu, *J. Phys. Chem. Lett.* 6 (2015) 2538–2545.